Differential Stability of Aurein 1.2 Pores in Model Membranes of Two Probiotic Strains

Galo E. Balatti[1]; Carmen Domene[2,3]; M. Florencia Martini[4,5] and Mónica Pickholz[1]*

[1.] Facultad de Ciencias Exactas y Naturales, Departamento de Física, Universidad de Buenos Aires, Argentina. CONICET-Universidad de Buenos Aires, IFIBA, Buenos Aires C1428BFA, Argentina.

[2.] Department of Chemistry, University of Bath, 1 South Bldg., Claverton Down, Bath BA27AY, The United Kingdom

[3.] Department of Chemistry, University of Oxford, Oxford OX1 3TA, Oxford, The United Kingdom

[4.] Universidad de Buenos Aires (UBA), Facultad de Farmacia y Bioquímica, Departamento de Farmacología, UBA, Junín 956, C1113AAD, Buenos Aires, Argentina

[5.] Instituto de Química y Metabolismo del Fármaco, Fac. de Farmacia y Bioquímica, (IQUIMEFA-UBA-CONICET), Junín 956, C1113AAD, Buenos Aires, Argentina

ABSTRACT

Aurein 1.2 is an antimicrobial peptide from the skin secretion of an Australian frog. In previous experimental work, we reported a differential action of aurein 1.2 on two probiotic strains *Lactobacillus delbrueckii subsp. Bulgaricus* (CIDCA331) and *Lactobacillus delbrueckii subsp. Lactis* (CIDCA133). The differences found were attributed to the bilayer compositions. Cell cultures and CIDCA331-derived liposomes showed higher susceptibility than the ones derived from the CIDCA133 strain, leading to content leakage and structural disruption. Here, we used Molecular Dynamics simulations to explore these systems at atomistic level. We hypothesize that if the antimicrobial peptides organized themselves to form a pore, it will be more stable in membranes that emulate the CIDCA331 strain than in those of the CIDCA133 strain. To test this hypothesis, we simulated pre-assembled aurein 1.2 pores embedded into bilayer models that emulate the two probiotic strains. It was found that the general behavior of the systems depends on the composition of the membrane rather than the pre-assemble system characteristics. Overall, it was observed that aurein 1.2 pores are more stable in the CIDCA331 model membranes. This fact coincides with the high susceptibility of this strain against antimicrobial peptide. In contrast, in the case of the CIDCA133 model membranes, peptides migrate to the water-lipid interphase, the pore shrinks and the transport of water through the pore is reduced. The tendency of glycolipids to make hydrogen bonds with peptides destabilize the pore structures. This feature is observed to a lesser extent in CIDCA 331 due to the presence of anionic lipids. Glycolipid transverse diffusion (flip-flop) between monolayers occurs in the pore surface region in all the cases considered. These findings expand our understanding of the antimicrobial peptide resistance properties of probiotic strains.

INTRODUCTION

The study of factors that affect the viability of probiotic cells is of particular interest in food and health sciences. Probiotics are living bacteria cells that confer health benefits to their host.[1] In humans, the intestinal tract hosts a plethora of probiotics that exert beneficial effects on our digestive and immune systems.[2] *Lactobacillus delbrueckii subsp. Lactis* (CIDCA133), which is able to counteract the action of pathogenic microorganims[3–6], protect intestinal mucose[7] or stimulate phagocytosis[8] is among this type of bacteria. CIDCA133 *in vitro* experiments have shown its resistance to cationic extracts of cultured human enterocytes and to antimicrobial peptides (AMPs) such as beta-defensins, present in the gastrointestinal tract.

AMPs are molecules found in virtually all domains of life. They have activity against a wide variety of biological membranes, and they are important components of innate immunity in vertebrate and invertebrate systems. They display remarkable structural and functional diversity with the ability to either kill microbial pathogens directly or act indirectly by modulating the host defense systems.[9–11] The overall mechanism of action described for most of the AMPs is based on their interaction with plasmatic membranes, where they can alter the physical integrity of the bacterial cell membrane at different degrees.[12–16] However, other ways of action of AMPs are reported in the literature, many of which affect membrane-associated biosynthesis or the interaction with intracellular targets [17,18]

Generally, AMPs are short cationic peptides (<40 aminoacids), with a net charge ranging from +1 to +9.[12,19] They adopt alpha-helix, beta-strand, loop or extended conformations, and they are classified into four categories according to their secondary structure.[12] The first group encompasses peptides that in solution display random coil conformations but they reorganize in

alpha-helical structures when they interact with lipid bilayers. Aurein 1.2, with sequence GLFDIIKKIAESF-NH2, belongs to this category and it is found in the skin of the Australian Tree Frogs[20]. It has a net positive charge and an overall hydrophobic moment of μH=6.77 in the Wimley-White interfacial hydrophobicity scale[21], calculated with the Totalizer module of the Membrane Protein Explorer software[22]. In its wild-type form, the C-terminus of aurein 1.2 is amidated by post-translational modification[20], which is a feature with relevance to its biological activity as it facilitates the interactions of the peptide with the lipid membrane[23]. The amphipathic character of aurein 1.2 is documented by circular dichroism (CD) experiments that have shown that aurein 1.2 adopts either an alpha-helical or random-coil conformation depending on whether it is in membrane or aqueous environment[24].

The mechanisms of action of aurein 1.2 are not entirely understood, and previous computational and experimental studies described different behavior of the peptide depending on the concentration and bilayer composition. It has been reported that the peptide can alter the target bilayer superficially, by interacting with lipid headgroups[25] and pulling out anionic lipids[26]; inducing reversible curvature in the membrane[27]; or promoting lateral segregation of anionic lipids, and thus, leading to membrane defects[28]. These surface effects of aurein 1.2 on bilayers could be concomitant with membrane leakage, which hinders the biological function of the membrane, and alters the cell viability[28]. The interaction of the peptide with the membrane surface can also result in a carpet-based mechanism triggered by a certain peptide concentration threshold that depends on the membrane composition[23,29,30]. Our previous computational studies of the ways of action of aurein 1.2 reported its capability to form pore structures[21,31]. In this respect, during evolution, prokaryotic cells have developed strategies to counteract antimicrobial

activity, and the bacterial response to antibiotic aggression is the prime example of bacterial adaptation, and the pinnacle of evolution. One of these strategies relies on the composition of the cell membrane, which dictates the peptide-lipid interaction.[32–34] It is exhaustively reported that some bacteria reduce their net surface charge, tempering the electrostatic interactions between the peptide and the cell membrane.[32–35] There are other properties of the bilayer associated with AMP resistance such as the increase of membrane fluidity or the negative curvature induced on the surface[27,36–39].

Aurein 1.2 interacts with some preference with bilayers composed of anionic over zwitterionic lipids. Specifically, mixtures of POPG:POPC vesicles were more vulnerable to the aurein 1.2 lytic action in comparison with pure POPC vesicles[30]; and Nuclear Magnetic Resonance (NMR) experiments showed a preferential interaction of aurein 1.2 with vesicles formed by mixtures of DMPC:DMPG in comparison with pure DMPC[24]. Likewise, negatively charged DMPG bilayers were perturbed to a greater extend by aurein 1.2 than neutral DMPC bilayers as shown by differential scanning calorimetry (DSC) experiments[40].

Recently, we reported that liposomes derived from the CIDCA133 strain are more resistant against the action of three anuran AMP peptides, citropin 1.1, maculatin 1.1 and aurein 1.2 than those from the CIDCA331 strain[41]. The CIDCA133 strain showed a greater minimal inhibitory concentration (MIC) and a remarkable cell viability (flow cytometry experiments) compared to the CIDCA331 strain,. In addition, the CIDCA133 was significantly inhibited by the three peptides in cell culture kinetics studies.[41] These observations suggest that the degree of resistance of the CIDCA133 strain to AMPs is higher compared to the CIDCA331 strain, both, in entire cells and CIDCA derived liposomes. Considering these observations, a plausible explanation for

the characteristic AMP-resistance of the CIDCA133 strain may be attributed to the membrane composition, and particularly, to a high carbohydrate content and fluidity as a result of a significant unsaturated lipid content. In this respect, the main differences between the CIDCA133 and CIDCA331 strands in terms of composition are the glycolipid/phospholipid ratio (GL/PL=23.33 for CIDCA133 and 3.08 for CIDCA331) and the degree of saturation of the lipid tails ($\%_{uns}$ of 70.2 and 42.8 respectively)[42–44].

Computer simulations are a powerful tool to characterize the mechanisms of interaction of AMPs with model membranes, and many studies have been already reported in the literature.[33,45–48] Previously, we used Molecular Dynamics (MD) simulations at the coarse grain level to explore the interactions of aurein 1.2 with eukaryotic[21] and prokaryotic[31] model membranes. These studies were further extended to investigate the nature of transient aurein pores in membranes with different GL/PL ratio[49].

In the present study, extensive all-atom MD simulations have been performed to assess the stability of pre-assembled pores of aurein 1.2 in model membranes of the CIDCA133 and the CIDCA331 strains to shed light into the differential experimental susceptibility that we observed between strains.

METHODOLOGY

Model Membranes

The membrane composition of the models was selected based in experimental data available for the CIDCA331 and the CIDCA133 strains.[42–44] A summary is presented in Table 1. The model membranes were composed of: 1-palmitoyl-2-oleoyl-sn-glycero-3-phospho-(1'-rac-glycerol) (POPG) and cardiolipin (CL2) with net charges of -1 and -2, respectively, and dioleoyl-3-monogalactosyl-sn-glycerol (DOMG) or 1-palmitoyl-2-oleoyl-3-monogalactosyl-sn-glycerol

(OPMG) in the **C133** and **C331** models, respectively. Chemical formulas of these molecules are depicted in Figure 1.

TABLE 1. Composition of the model membranes considered in this study

	Membrane Composition		
System	Glycolipids	Phospholipids	
		POPG	CL2
C331	384 OPMG (75%)	96 (18.75%)	32 (6.25%)
C133	490 DOMG (96%)	14 (3%)	4 (1%)

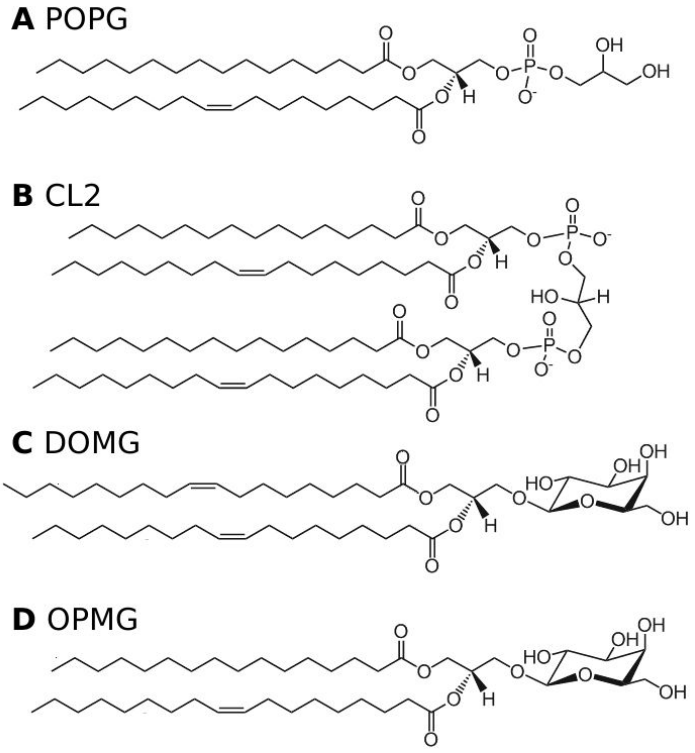

Figure 1: Chemical structures of the lipids considered in the compositions of **C133** and **C331** model membranes: (A) POPG, (B) CL2, (C) DOMG and (D) OPMG.

Pore assembly

The aurein1.2 structure obtained from NMR experiments[20] (code 1VM5) was retrieved from the Protein Data Bank[50]. The ionization states corresponding to neutral pH, the natural form of the peptide, were considered for all the amino acids, with the C-terminal amidated and the N-terminal protonated.

In previous CG simulations, aurein 1.2 formed pores structures composed of 16 peptides on average per pore, that had well-defined characteristics such as the disposition of molecules per leaflet with a preferential 35° tilt angle with respect to the membrane normal in agreement with NMR experimental observations[51]. It was observed that the amidated termini were oriented toward the hydrophobic core of the bilayer whilst the amine termini were oriented toward the membrane interphase[21,31]. Based on this prior computations, two types of pores consisting of 16 aurein 1.2 molecules were built with at atomistic level with identical characteristics (Figure 2A).

One of the pore structures considered, **M**, corresponds to a structure where the polar side of the peptides faces the pore interior (Figure 2B). In previous simulations, this type of pores self-assembled to render a structure with hydrophilic residues organized to face a cavity filled with water molecules, and the hydrophobic residues facing the lipid tails. An alternative pore structure, **FW,** considered to evaluate the relevance of the orientation, corresponds to a pore where all the peptide molecules are translated in the xy plane without involving any rotation (see were oriented perpendicular to the bilayer and inserted into the two model membranes considered. The initial diameter of the pore structures was 3.0-3.5 nm. The bilayer were composed of 512 lipids and the peptide:lipid (P:L) ratio was 1:32, in line with the literature and our previous studies[21,30,31]. In addition, peptides were placed in the aqueous solution at 3 nm far from the interphase with a **C331** model membrane. This case is referred as the **331S** system. Two

bilayers without peptides were also considered and referred as **N**. A summary of the systems examined is presented in Table 2.

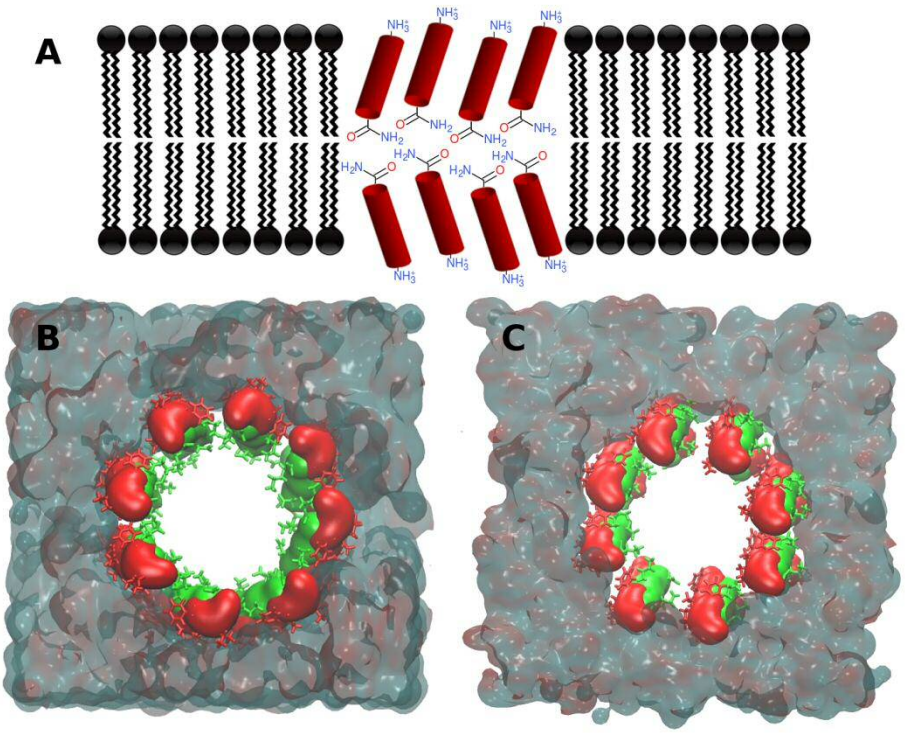

Figure 2: (A) Cartoon representation of the distribution of aurein 1.2 peptides in the lipid membrane. Initial structural organization of the pore for the (B) **M** and (C) **FW** systems. Polar and charged peptide surfaces are depicted in green and the non-polar ones are in red.

In what follows, the identification number of the strains and the initial pore conformation identifier will be used to denominate each system considered. For example, **331M** refers to pore type **M** embedded in a **C331** bilayer.

System setup

The *membrane builder* module of CHARMM-GUI (http://www.charmm-gui.org/) was employed to generate the membranes and insert the pore structures into them using in-house scripts. The *solvate* CHARMM-GUI module was used to achieve a final concentration of 0.1 M NaCl. MD simulations were performed with the GROMACS 2018.3[52–56] software package. CHARMM36[57] parameters were used for ions, phospholipids, glycolipids and aminoacids, and the TIP3P model was used for water molecules.

The Particle Mesh Ewald method (PME)[58] was used for the treatment of periodic electrostatic interactions with a cut-off distance of 1.2 nm. The Lennard-Jones potential was smoothed over the cut-off range of 1.0-1.2 nm by using the force-based switching function. Only atoms in the Verlet pairs list with a cut-off range reassigned every 20 steps were considered. The LINCS[59] algorithm was used to constrain all bonds involving hydrogen atoms to allow the use of a 2 fs time step. The protocol; suggested by Lee *et al*[60] for non-bonded interactions with the CHARMM36 forcefield when used in the GROMACS suite was followed.

The systems were equilibrated in six stages with the peptides and lipids restrained using different force constants and relaxed progressively until the lipids are let free to move around a softly restrained protein backbone. The first 20 ns of the production run were discarded as part of the equilibration protocol. Production runs were performed in a $NP_{XY}P_ZT$ *ensemble*. The temperature was maintained at 310 K with the Nose-Hoover thermostat[61,62] using a time constant of 1.0 ps. The pressure was maintained at 1 bar with the semi-isotropic Parrinello-Rahman barostat[63] using a compressibility of 4.5×10^{-5} bar^{-1} and a time constant of 1.0 ps in a rectangular simulation box. The simulation protocol employed is summarized in Table S2 of the SI.

Trajectory analysis

Mass density profiles (MDPs) and density maps were calculated with the *gmx density* and *gmx densmap* tools from the GROMACS package. To quantify the content of peptide, water and galactose inside the bilayer, a "hydrophobic region" between -1 and +1 nm from the bilayer center was defined, and the MDP density of these regions was calculated. The errors bars were obtained by calculating the differential permeation at 0.1 nm outside and inside of the hydrophobic region limits. The total number of hydrogen bonds was calculated using the *hbonds* VMD plugin, using a distance of 3Å and an angle of 30 degrees to define the hydrogen bond.

TABLE 2. Summary of the systems considered in this study and their composition.

System Name	System Composition	Time (ns)
331N	384 OPMG : 96 POPG : 16 CL2 : 18052 TIP3 : 158 Na^+ : 30 Cl^-	1000
133N	490 DOMG : 16 POPG : 3 CL2 : 17985 TIP3 : 67 Na^+ :45 Cl^-	1000
331M	384 OPMG : 96 POPG : 16 CL2 : 46452 TIP3 : 214 Na^+ : 102 Cl^- : 16 peptides	2300
133M	490 DOMG : 16 POPG : 3 CL2 : 46356 TIP3 : 107 Na^+ : 101 Cl^- : 16 peptides	2300
331FW	384 OPMG : 96 POPG : 16 CL2 : 18529 TIP3 : 161 Na^+ : 49 Cl^- : 16 peptides	2300
133FW	490 DOMG : 16 POPG : 3 CL2 : 20097 TIP3 : 58 Na^+ : 52 Cl^- : 16 peptides	2300
331S	384 OPMG : 96 POPG : 16 CL2 : 46324 TIP3 : 214 Na^+ : 102 Cl^- : 16 peptides	2400
Total Simulation Time		13600

RESULTS AND DISCUSSION

The goal of this study was to understand from an atomistic point of view the differential susceptibility of the CIDCA133 and CIDCA331 strains to the AMP aurein 1.2. This phenomenon was observed experimentally in both, living cells and bacterial-derived liposomes[41]. The higher susceptibility of CIDCA331 to aurein 1.2 was ascribed in part to its membrane composition[42]. Our hypothesis is that if a pore is formed, it will be more stable in a model membrane that emulates the CIDCA331 strain rather than one that emulates the CIDCA133 membrane. To test this hypothesis and to characterize the stability of pre-assembled aurein 1.2 pore structures embedded in two types of bilayers emulating the CIDCA331 and CIDCA133 probiotic strains, extensive atomistic MD simulations amounting 13.6 μs were performed were performed.

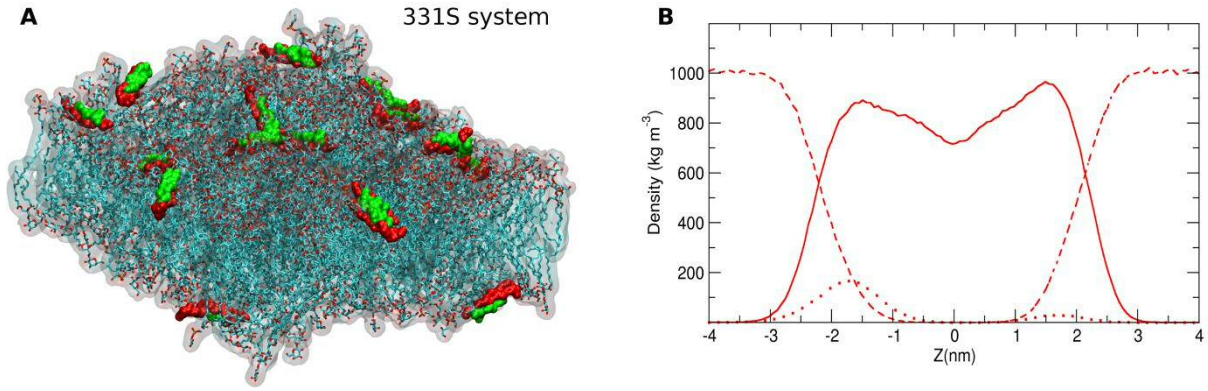

Figure 3: (A) Snapshot of the last frame (2.3 μs) of the **331S** system. Polar and charged peptide surfaces are depicted in green, and non-polar surfaces are shown in red. Lipids are represented with sticks with a ghost surface representation. (B) Mass density profiles of water (dashed line), lipids (solid line) and peptides (dotted line) averaged over the last 500 ns of the simulations for the **331S** system.

Firstly, the **331S** system, where the peptides are initially placed in the aqueous solution in the vicinity of a model **C331** bilayer a 2.4-μs simulation was considered. As expected, pore

formation did not realised at this time scale, and instead, the peptides were adsorbed at the water-lipid interphase (Figure 3A), as already reported in the literature for other peptides[28,64] The peptide distribution at the water/lipid interphase is shown in Figure 3. According to mathematical studies of penetration, the size of the peptide (> 9 residues) and its physicochemical characteristics could lead to its insertion in mixture membranes[65]. Their results indicate that peptides preconcentrate on the surface of intact lipid mixture before jumping across it.

The time evolution of pre-assembled pore structures was followed. It has been found out that evolution of the specific properties studied are dependent on the composition of the membrane considered rather than the initial organization of the pre-assembled pore. The peptide pores were stabilized by hydrogen bonds established between the peptides and peptides with the water molecules inside the pores. Glycolipids played an important role by filling the pore fenestrations. Those peptide regions are suitable for binding polar galactose moieties, attracting them to the inner core of the membrane.

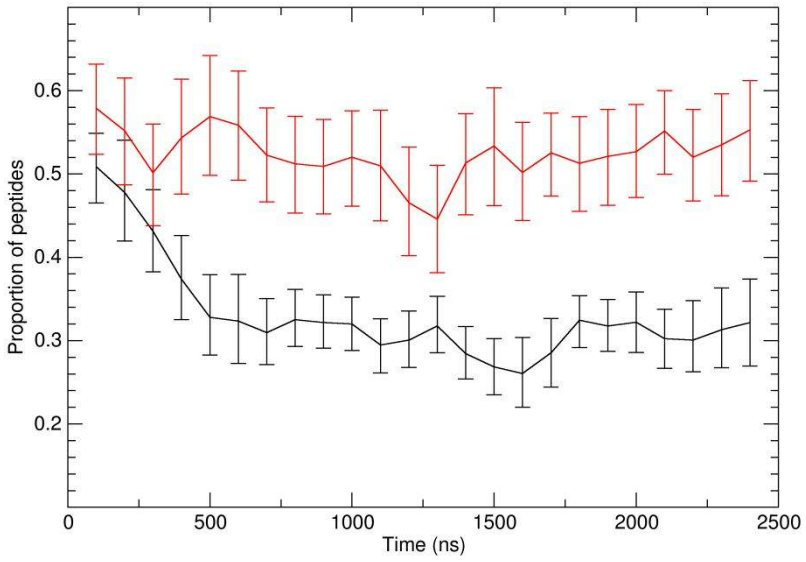

Figure 4: Proportion of peptides inside the hydrophobic core of the lipid membrane with respect to the total number of peptides in the simulation system as a function of the simulation time. The red and black traces correspond to the **331M** and **133M** systems, respectively.

The evolution of the number of peptides in the inner core of the bilayer as function of the time for the **M** systems is shown in Figure 4. The number of peptides that constitute the pore remains constant during the simulation in the **331M** case which is at odds with the behavior of the peptides in the **133M** case where the proportion of peptides smoothly decreased during the first 600 ns of the simulations. In this way, the pore seems to be more stable in the **C331** bilayer than in the **C133** one. This could partially explain the susceptibility of **C331** bilayers to the aurein 1.2 action[41]. Migration of individual peptides from the pore to the interphase was observed, especially in **C133** bilayers. Once a peptide moves to the interphase, it stays there for the remaining simulation, as reported in similar studies[21,27,31]. Furthermore, the peptides at the surface do not aggregate but instead, they are adsorbed in the bilayer with the polar sidechains oriented toward the water phase. Previously, similar aurein 1.2 behavior was reported from coarse grain MD simulations studies.[21,31]

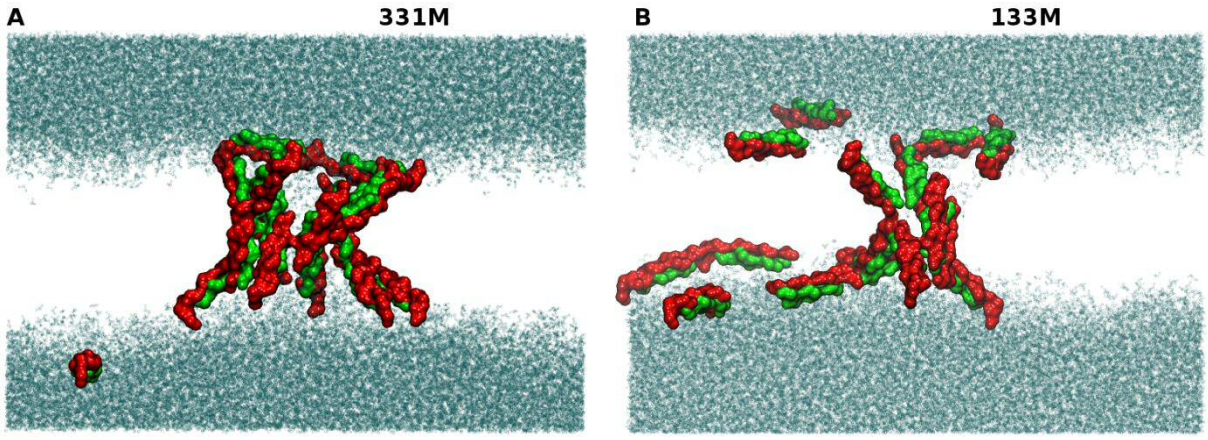

Figure 5: Representative snapshots at 2.2 μs of the (A) **331M** and (B) **133M** systems. Polar and

charged peptide surfaces are depicted in green, and non-polar surfaces are shown in red. Water molecules are represented in cyan and the lipid bilayer is not shown for clarity.

The final representative structures of the pores in the simulations with bilayers **133M** and **331M** are illustrated in Figure 5. Despite the pore conformation was the same at the start of the simulation, the stability of the pore structure depends on the lipid composition; the **331M** pore is stable in stark contrast with the **133M** pore. In the later system, several aurein 1.2 peptides moved from the peptide assembly toward the interphase. Peptides in the **331FW** and **133FW** systems display generally the same behavior than those in the **331M** and **133M** systems, respectively. Nevertheless, the aurein 1.2 molecules rotated to align their polar faces towards the interior of the pore resembling the **331M** structure in the case of **331FW**. This configuration enhanced the interaction with the water molecules inside the pore and stabilized its overall structure. In the **133FW** case, some of the peptides migrate to the water-membrane interphase, like in the **133M** case, but they induce a curvature in the bilayer.

Further information about the overall organization of the bilayers was obtained through the MDPs. The MDPs of the lipids and water in the **331N** and **133N** systems are shown in Figure 6.A. Well defined bilayers characterized by different degrees of thickness are found in the **N** systems. The thickness is defined as the distance between peaks in the total lipid density: 3.4±0.1 nm and 3.0±0.1 nm for **331N** and **133N**, respectively. These data together with the valley-to-peak ratio, deeper in the **331N** system, reveals a higher degree of organization in the **331N** bilayer in comparison to the **133N** system. This observation is expected if we consider the presence of glycolipids with a lower degree of tail unsaturation. Likewise, the average lipid area was found to be 57.8±0.6 $Å^2$ for the **331N** system compared to 64.9±0.7 $Å^2$ for **133N**.

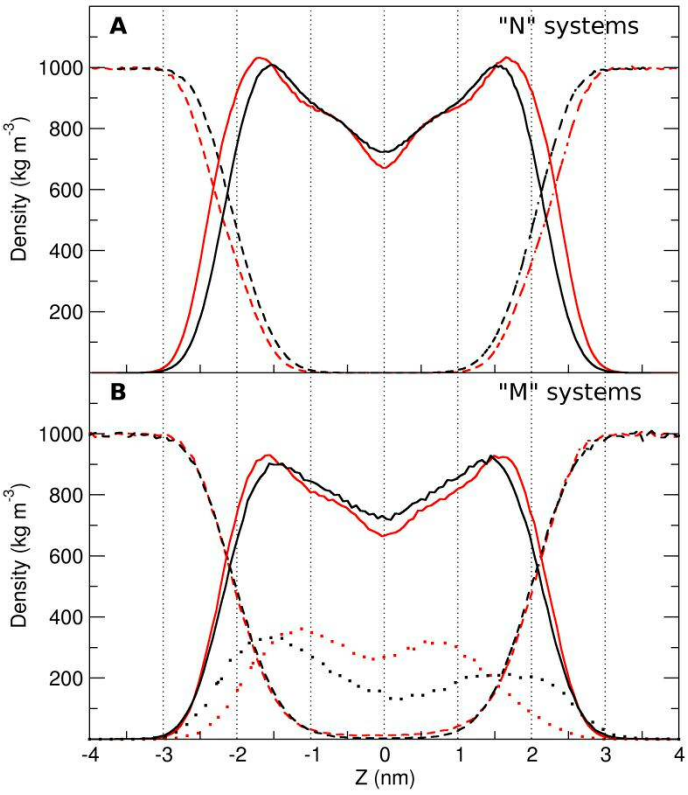

Figure 6: Mass density profiles for water (dashed line), lipids (solid line) and peptides (dotted line) averaged over the last 500 ns of the simulations for (A) **N** and (B) **M** systems. Red and black traces represent **C331** and **C133** systems, respectively. Peptide densities are magnified five times for clarity.

The water, total lipids and peptides MDPs for the **M** systems is shown in Figure 6.A. In the presence of the pore, there is no significant difference between the thickness of the **331M** or **133M** bilayers, 3.1±0.1 and 3.0±0.1 nm respectively. This suggests different organization, in particular in the **C331** bilayers. The peptide distribution confirms the difference in the pore assembly organization within the bilayer. Comparing the distribution of the peptides in each bilayer, inside the **331M** bilayer, it is more uniform and denser compared to the 113M case where more peptides are found at the interphase. In contrast to what it is observed in well-

organized lipid membranes, the density of water is not negligible in the hydrophobic core regions as it was already described in other simulation studies of pore-like structures[66]. The MDPs of all the systems considered are presented in SI (figures S2-S6).

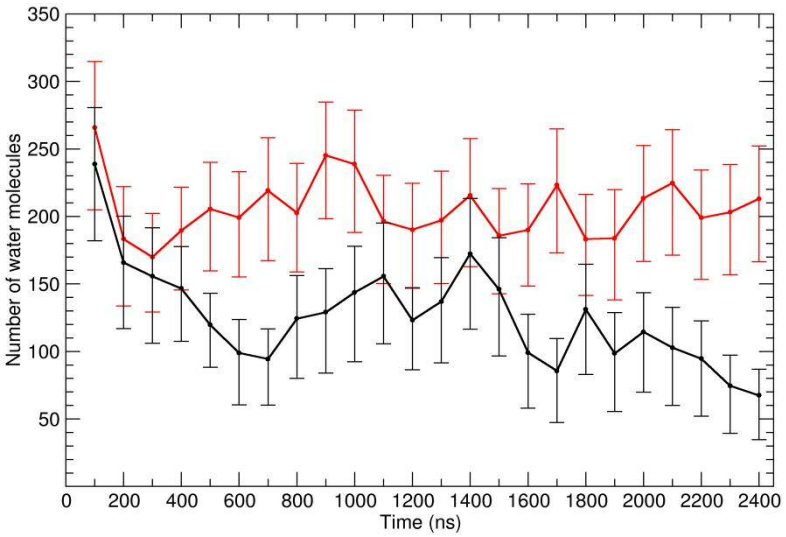

Figure 7: Number of water molecules inside the hydrophobic core of the lipid membrane as a function of simulation time. The red and black traces correspond to the **331M** and **133M** systems, respectively

The biological activity of these peptide structures relies on the transport of water through them. Indeed, water molecules were found inside the bilayer center when peptides were organized forming a pore inside the bilayer. Figure 7 shows the evolution of the number of water molecules in the inner core of the bilayer as a function of time for the **M** cases. The amount of water inside the pore remains stable for the **331M** system but it decreases for the **133M** system. The pore structure in **331M** remains stable and water can easily permeate throw it. In contrast, peptides migrated toward the interphase of the bilayer in the **133M** case and in parallel, the pore structure closes. This tendency was also observed in the **133FW** and **331FW** systems with some peculiarities. For instance, at the beginning of the simulations, some of the peptides oriented

their polar regions toward the lipid hydrophobic tails, and as a result, the **FW** pores are less stable than the **M** ones. A slow spin of the peptides, that first increased the pore diameter with the concomitant water access permeation, was observed in **331FW** (Figures S6A and S6B). This was followed by a pore relaxation resulting in a more organized and stable structure. The number of water molecules inside the pore decreases in the **133FW** system as illustrated by the snapshots of Figure 8. As a result of the peptide organization, the membrane curvature changes, and the exact quantification of the number of water molecules is not viable.

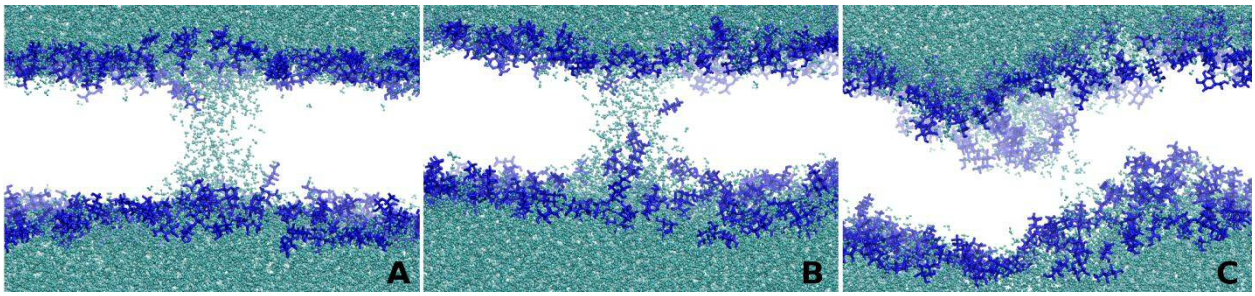

Figure 8: Snapshots of the **133FW** system at (A) the beginning of the simulation t=0, (B) t=950 ns and (C) at the end of the simulation, t=2200 ns. Water is represented in cyan and galactose in blue.

In addition to the water flux, galactose headgroups are found inside the bilayer in the pore region. The evolution of the number of galactose molecules in the inner core of the bilayer as a function of time for the **M** cases is shown in Figure 9. The **331M** system, with a stable pore, shows, approximately, four galactose groups inside the hydrophobic region. In the case of **133M**, the number of sugars in this region increases, reaching a maximum value of ~19. This value decreases in parallel with the decrease of the size of the pore. Similar results were obtained for the **FW** systems, but the membrane ripples make difficult its estimation. The polar faces of the peptide structures are responsible for the presence of the galactose moieties in this region. Once there, they seem to promote the pore destabilization process by weakening peptide-peptide

interactions. Considering that the two membranes have a high percentage of glycolipids, the difference in phospholipids may be the key in the differential stability.

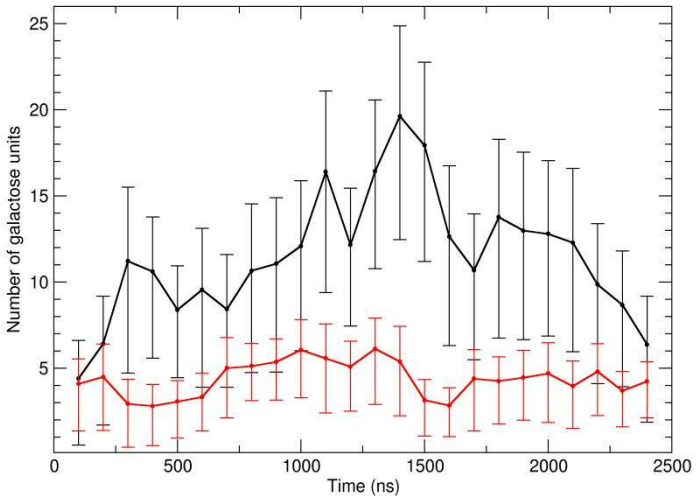

Figure 9: Number of galactose units inside the hydrophobic core of the lipid membrane as a function of simulation time. The red and black traces correspond to the **331M** and **133M** systems respectively

To further characterize the contribution of galactose to AMP-resistance, the number of hydrogen bonds (HB) between galactose and the peptides was analyzed as a function of simulation time. Galactose establishes 4±2 and 6±2 hydrogen bonds with the peptides in the **331M** and **331FW** systems respectively (Figure 10A)**.** The number remains constant during the simulation which can be associated with the degree of pore stability in **C331** membranes. In contrast, the number of hydrogen bonds when peptides are at the water-membrane interphase is higher; for instance, the average is 13±1 in the **331S**, system (Figure S9).

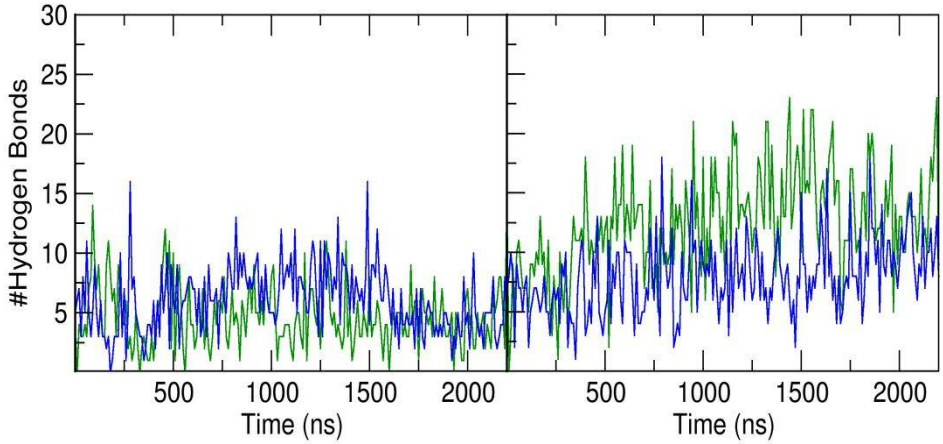

Figure 10: Number of hydrogen bonds (HB) formed between the galactose glycolipid headgroups and the peptides in the (A) **C331** and (B) **C133** membranes. Green and blue traces correspond to the **M** and **FW** systems respectively.

The HB time evolution for the **133M** and **133FW** systems is shown in Figure 10B. In both cases, the number of interactions increases with time despite starting at similar values. At the end of the simulation, at 2.3 μs, values in the range of 9-13 are reached. These results are compatible with what it is expected from the pore evolution. In the **C331** membrane, the pore remains assembled in a stable configuration, whilst in **C133** membranes, the number of hydrogen bonds increases accounting for the migration of the peptide to the bilayer interphase, with the consequent pore narrowing. From the analysis of the interactions between the peptides and the lipid headgroups, it was found that aspartic and glutamic residues contribute the most to the interactions, followed by serine and phenylalanine (Figure 11). Greater numbers of HB interactions are found in the **C133** membranes as a result of the migration of the peptides to the interphase, and the tendency of the glycolipids headgroups to penetrate the core of the membrane.

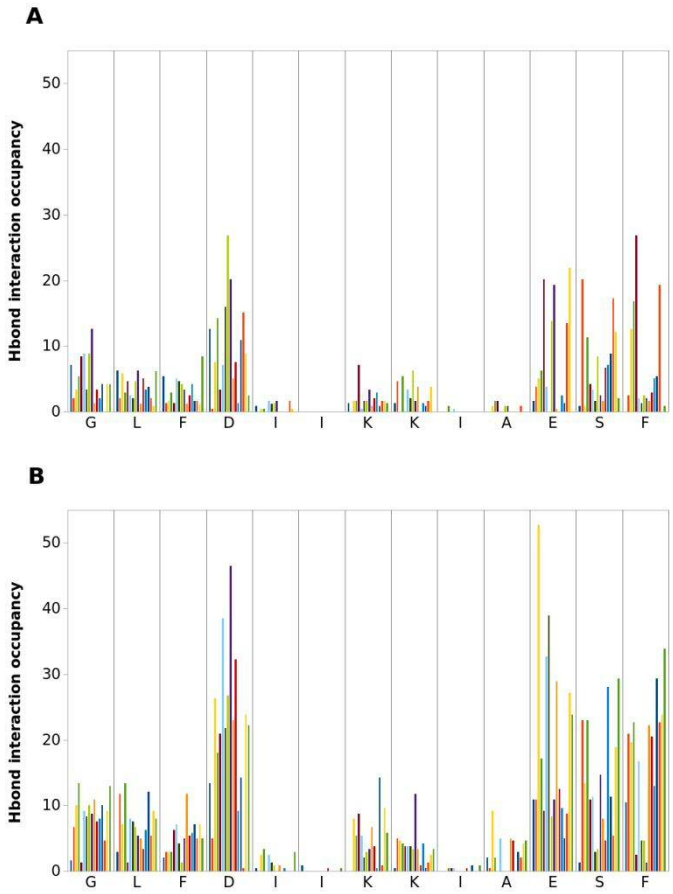

Figure 11: Occupancy percentage of peptide residues HB with lipid membrane groups. Each amino acid is expressed as one letter code, and there is one different color for the residue of each peptide. (A) **C331** and (B) **C133** systems.

Lipid flip-flops were evaluated by tracking the position of the ether oxygen atom of the galactose group for glycolipids and the phosphorous atom of the phosphate group of the phospholipids. At least one glycolipid flip-flop event was identified in each simulation, and none for phospholipids. The z trajectories of two selected glycolipid ether oxygen atoms undergoing flip-flop in opposite directions in the **331FW** system are shown in Figure 12A, Snapshots illustrating the flip-flop events in this simulation are shown in figures 12B-D. The glycolipids involved in the flip-flip event are localized at the bilayer center, with the saccharide groups

directly interacting with the peptides, and the tails oriented toward the acyl lipid chains and parallel to the plane of the bilayer.

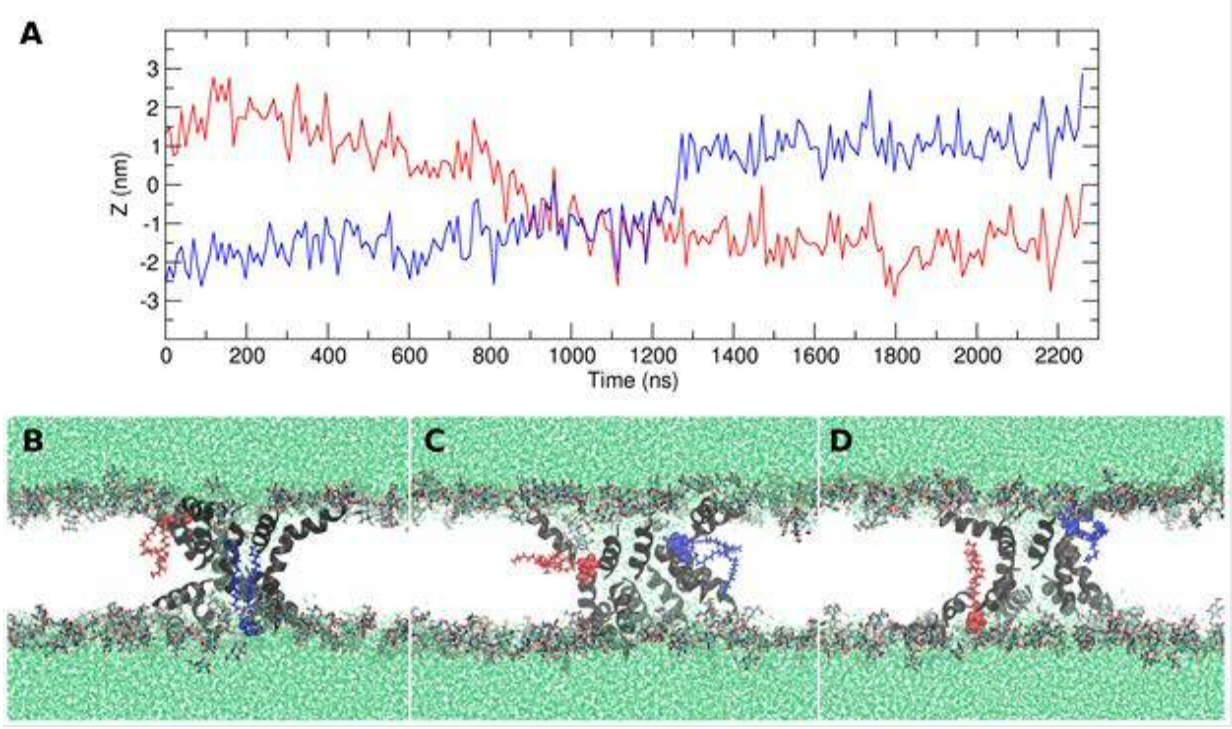

Figure 12: (A) Trajectories along the z-axis of ether oxygen atoms of the glycolipid headgroups of two selected molecules that participate in flip-flop events in the **331FW** system. Snapshots of the system at (B) 600 ns, (C) 1200 ns and (D) 2400 ns. Water is shown in green, bulk lipid headgroups in cyan/red, and peptides in cartoon representation in black

Phospholipids distribution in the xy plane could play an important role on the differential stability of the pore in C311 membranes. The density maps of the glycolipids and phospholipids were calculated and the backbone protein density map was used as a reference (Figure 13A). The glycolipid density map (Figure 13B) shows a wide homogeneous region (light green) that decreases in the vicinity of the pore (yellow and red). The phospholipid density map shows an uneven distribution with peptide accumulation at the edge of the pore (Figure 13C). In the **C331**

bilayer, the pore is surrounded by anionic phospholipids. Figures S10-S12 of SI show the density maps of the other cases.

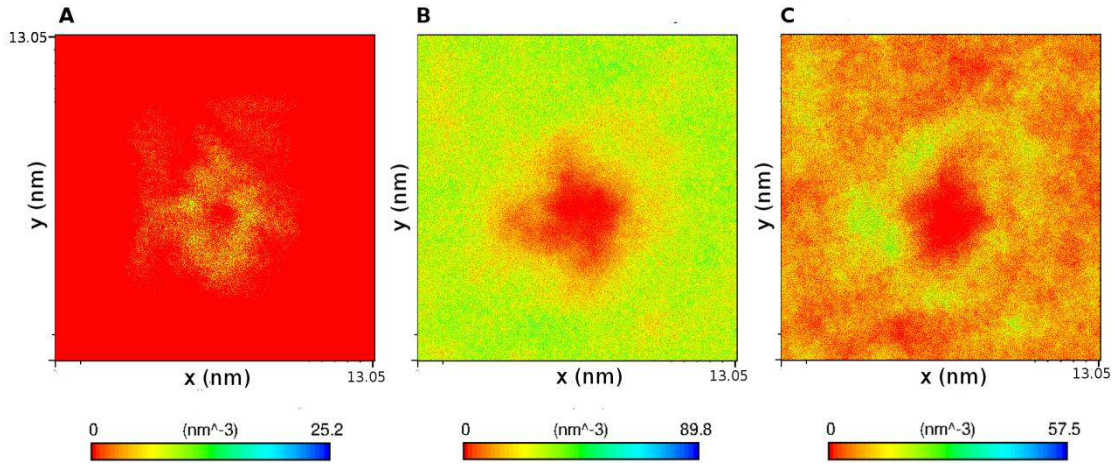

Figure 13: Density maps for (A) peptide backbones, (B) glycolipids and (C) phospholipids in the xy plane of the **331M** bilayer. Red represents the absence of molecules

The radial distribution function, g(r), calculated between the phosphorous atoms of the phosphate groups of the phospholipids and the nitrogen atoms of either the side chain of lysine or the terminal group of glycine in the **331M** and the **331FW** systems is shown in Figure 14. A well-defined first peak at a ~4Å, characteristic distance of salt bridges interactions, is observed[67]. The interactions between peptides and charged phospholipids that could be partially responsible for maintaining the pore architecture were identified as salt bridges between these groups.

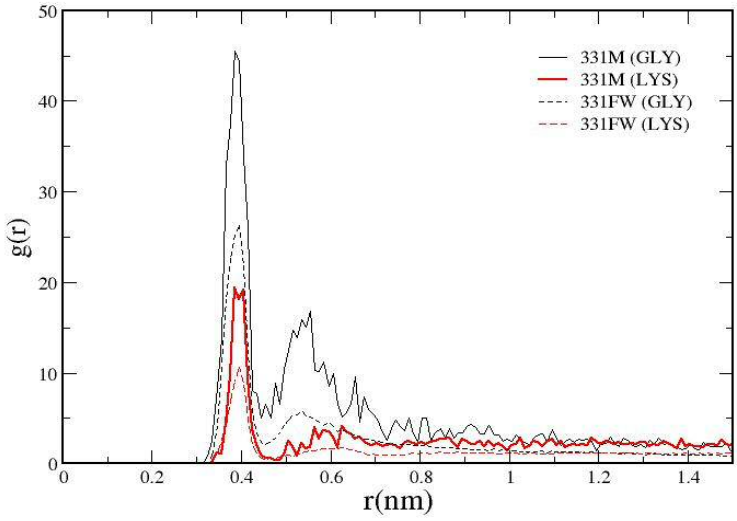

Figure 14: Radial distribution function between the phosphorous of the phospholipids and the amine nitrogen of the peptide terminal glycine (in black) and the side chain lysine nitrogen (red). Solid and dashed lines are used for **M** and **FW** systems, respectively.

CONCLUSIONS

The aim of this work was to explore the mechanism of action of antimicrobial peptides in model membranes of two specific probiotic strains. We focused on the stability of the pre-assembled peptide pores in two model membranes. Considering our previous experimental findings and those by others, we expected greater stability in membranes that emulate the CIDCA331 strain compared to those in the CIDCA133 one. Our results are consistent with experimental reports on whole bacteria (CIDCA strains 331 and 133) and liposomes formed by lipids extracted from the aforementioned strains[41] In both cases, a greater susceptibility of strain 331 was observed with respect to the 133 strain against the action of aurein 1.2. In these experiments, the minimum inhibitory concentration (MIC) values for the CIDCA133 strain were doubled those of the CIDCA331 strain. The CIDCA133 strain was able to grow at sub-MIC concentrations (12 μM) of aurein 1.2, while CIDCA331 was significantly inhibited under the

same conditions. Equally, the release of carboxyfluorescein of LUV at low concentrations is quantitatively higher for CIDCA331 vesicles compared to CIDCA133 ones, and the same was observed in GUV with fluorescence microscopy[41]. Likewise, our own computational CG simulation studies on prokaryotic model membranes[21,31] provided insigs into self-assembly and the formation of peptide pores. In this context, our hypothesis was formulated.

Our results show that the composition of the membrane is a crucial factor for the pore stability. The pores remain stables in the model membranes corresponding to CIDCA331. However, some peptides migrated to the surface in the simulation of the CIDCA133 system. Our results suggest that if a pore is formed by any mechanism, it will be more stable in the CIDCA331 rather than in CIDCA133 membranes. The mechanism by which the pore closes may be associated to the presence of a high number of glycolipids, present in both strains. The galactose unit has four hydroxyl groups, which are potential donor-acceptor of hydrogen atoms to establish specific interactions. However, the CIDCA331 strain contains a higher percentage of negatively charged lipids (POPG and CL2). These anionic lipids surround the pore shielding it from the glycolipid action. Further studies need to explore the transient aurein 1.2 pore lifetime as a function of the number of anionic phospholipids. A possible factor to be exploited to enhance or avoid the action of AMPs like aurein 1.2 is the presence of glycolipids.

This piece of work provides insight about the molecular host-probiotic interactions. Several beneficial effects of probiotic microorganisms have been described in the literature[1,68–71]. However, their mechanisms of action are diverse, heterogeneous, strain specific, and still not entirely understood[72] . Computer simulation studies, like the ones presented here, help to shed light on some of these aspects to maximize their applications in healthcare and food industries.

ASSOCIATED CONTENT

Supporting Information.

The following files are available free of charge.

- More information about CIDCA133/CIDCA331 lipid composition, the equilibration protocol, snapshots and mass density profiles of all the systems, number of hydrogen bonds (331S system) and density maps (133M, 331FW and 133FW systems) (PDF).

AUTHOR INFORMATION

Corresponding Author

* Author to whom correspondence should be addressed: mpickholz@df.uba.ar

Author Contributions

G.E.B. performed the simulations. All the authors were involved in the analysis and discussion of the data as well as in writing the article.

Funding Sources

Argentina National Scientific and Technical Research Council (CONICET).

Grants: ANPCyT (PICT 2013-1205; PICT 2014-3653).

ACKNOWLEDGMENT

C.D. acknowledges the Partnership for Advanced Computing in Europe (PRACE) for an award to access computational resources in Daint at the Swiss National Supercomputing facility (https://www.cscs.ch/).

ABBREVIATIONS

CIDCA 133, Lactobacillus delbrueckii subsp. Lactis; CIDCA 331, L. delbrueckii subsp. Bulgaricus; CL2, 1',3'-bis[1-palmitoyl-2-oleoyl-sn-glycero-3-phospho]-glycerol; CG, Coarse Grain; DMPC, 1,2-dimyristoyl-sn-glycero-3-phosphocholine; DMPG, 1,2-dimyristoyl-sn-glycero-3-phospho-(1'-rac-glycerol); DOMG, 1-palmitoyl-2-oleoyl-3-monogalactosyl-sn-glycerol; FW, Ferris Wheel; HB, Hydrogen bonds; M, Moon; MDP, mass density profile; MD, Molecular Dynamics; N, Neat; OPMG, dioleoyl-3-monogalactosyl-sn-glycerol; PME, particle mesh Ewald method; POPG, 1-palmitoyl-2-oleoyl-sn-glycero-3-phospho-(1'-rac-glycerol); S, Surface.

REFERENCES

(1) Hotel, A.; Cordoba, A. Health and Nutritional Properties of Probiotics in Food Including Powder Milk with Live Lactic Acid Bacteria. *Prevention* **2001**.

(2) Savage, D. C. Microbial Ecology of the Gastrointestinal Tract. *Annu. Rev. Microbiol.* **1977**. https://doi.org/10.1146/annurev.mi.31.100177.000543.

(3) Kociubinski, G. L.; Pérez, P. F.; Añón, M. C.; De Antoni, G. L. A Method of Screening for Highly Inhibitory Lactic Acid Bacteria. *J. Food Prot.* **1996**. https://doi.org/10.4315/0362-028X-59.7.739.

(4) Kociubinski, G.; Pérez, P.; De Antoni, G. Screening of Bile Resistance and Bile Precipitation in Lactic Acid Bacteria and Bifidobacteria. *J. Food Prot.* **1999**. https://doi.org/10.4315/0362-028X-62.8.905.

(5) Hugo, A. A.; Kakisu, E.; De Antoni, G. L.; Pérez, P. F. Lactobacilli Antagonize Biological Effects of Enterohaemorrhagic Escherichia Coli in Vitro. *Lett. Appl. Microbiol.* **2008**. https://doi.org/10.1111/j.1472-765X.2008.02363.x.

(6) Hugo, A. A.; De Antoni, G. L.; Pérez, P. F. Lactobacillus Delbrueckii Subsp Lactis Strain CIDCA 133 Inhibits Nitrate Reductase Activity of Escherichia Coli. *Int. J. Food Microbiol.* **2006**. https://doi.org/10.1016/j.ijfoodmicro.2006.04.024.

(7) De Jesus, L. C. L.; Drumond, M. M.; de Carvalho, A.; Santos, S. S.; Martins, F. S.; Ferreira, Ê.; Fernandes, R. S.; de Barros, A. L. B.; do Carmo, F. L. R.; Perez, P. F.; Azevedo, V.; Mancha-Agresti, P.. Protective Effect of Lactobacillus Delbrueckii Subsp. Lactis CIDCA 133 in a Model of 5 Fluorouracil-Induced Intestinal Mucositis. *J. Funct. Foods* **2019**. https://doi.org/10.1016/j.jff.2018.12.027.

(8) Hugo, A. A.; Rolny, I. S.; Romanin, D.; Pérez, P. F. Lactobacillus Delbrueckii Subsp. Lactis (Strain CIDCA 133) Stimulates Murine Macrophages Infected with Citrobacter Rodentium. *World J. Microbiol. Biotechnol.* **2017**. https://doi.org/10.1007/s11274-017-2219-4.

(9) Wang, G.; Li, X.; Wang, Z. APD3: The Antimicrobial Peptide Database as a Tool for Research and Education. *Nucleic Acids Res.* **2016**, *44* (D1), D1087-93. https://doi.org/10.1093/nar/gkv1278.

(10) Reddy, K. V. R. R.; Yedery, R. D.; Aranha, C. Antimicrobial Peptides: Premises and Promises. *International Journal of Antimicrobial Agents*. **2004**, pp 536–547. https://doi.org/10.1016/j.ijantimicag.2004.09.005.

(11) Martin, E.; Ganz, T.; Lehrer, R. I. Defensins and Other Endogenous Peptide Antibiotics of Vertebrates. *J. Leukoc. Biol.* **1995**, *58*, 128–136.

(12) Jenssen, H.; Hamill, P.; Hancock, R. E. W. Peptide Antimicrobial Agents. *Clinical Microbiology Reviews*. **2006**, pp 491–511. https://doi.org/10.1128/CMR.00056-05.

(13) De La Fuente-Núñez, C.; Cardoso, M. H.; De Souza Cândido, E.; Franco, O. L.; Hancock, R. E. W. Synthetic Antibiofilm Peptides. *Biochim. Biophys. Acta - Biomembr.* **2016**. https://doi.org/10.1016/j.bbamem.2015.12.015.

(14) Dathe, M.; Wieprecht, T. Structural Features of Helical Antimicrobial Peptides: Their Potential to Modulate Activity on Model Membranes and Biological Cells. *Biochim. Biophys. Acta - Biomembr.* **1999**, *1462*, 71–87. https://doi.org/10.1016/S0005-2736(99)00201-1.

(15) Huang, Y.; Huang, J.; Chen, Y. Alpha-Helical Cationic Antimicrobial Peptides: Relationships of Structure and Function. *Protein Cell* **2010**, *1*, 143–152. https://doi.org/10.1007/s13238-010-0004-3.

(16) Hancock, R. E. W.; Rozek, A. Role of Membranes in the Activities of Antimicrobial Cationic Peptides. *FEMS Microbiology Letters*. **2002**, pp 143–149. https://doi.org/10.1016/S0378-1097(01)00480-3.

(17) Haney, E. F.; Straus, S. K.; Hancock, R. E. W. Reassessing the Host Defense Peptide Landscape. *Frontiers in Chemistry*. **2019**. https://doi.org/10.3389/fchem.2019.00043.

(18) Raheem, N.; Straus, S. K. Mechanisms of Action for Antimicrobial Peptides With Antibacterial and Antibiofilm Functions. *Frontiers in Microbiology*. **2019**. https://doi.org/10.3389/fmicb.2019.02866.

(19) Tossi, A.; Sandri, L.; Giangaspero, A. Amphipathic, Alpha-Helical Antimicrobial Peptides. *Biopolymers* **2000**, *55*, 4–30. https://doi.org/10.1002/1097-0282(2000)55:1<4::AID-BIP30>3.0.CO;2-M.

(20) Rozek, T.; Wegener, K. L.; Bowie, J. H.; Olver, I. N.; Carver, J. A.; Wallace, J. C.; Tyler,. M. J. The Antibiotic and Anticancer Active Aurein Peptides from the Australian Bell Frogs Litoria Aurea and Litoria Raniformis: The Solution Structure of Aurein 1.2. *Eur. J. Biochem.* **2000**, *5341*, 5330–5341. https://doi.org/10.1046/j.1432-1327.2000.01536.x.

(21) Balatti, G.; Ambroggio, E.; Fidelio, G.; Martini, M.; Pickholz, M. Differential Interaction of Antimicrobial Peptides with Lipid Structures Studied by Coarse-Grained Molecular Dynamics Simulations. *Molecules* **2017**, *22*, 1775. https://doi.org/10.3390/molecules22101775.

(22) Snider, C.; Jayasinghe, S.; Hristova, K.; White, S. H. MPEx: A Tool for Exploring Membrane Proteins. *Protein Sci.* **2009**, *18*, 2624–2628. https://doi.org/10.1002/pro.256.

(23) Shahmiri, M.; Enciso, M.; Mechler, A. Controls and Constrains of the Membrane Disrupting Action of Aurein 1.2. *Sci. Rep.* **2015**. https://doi.org/10.1038/srep16378.

(24) Fernandez, D. I.; Le Brun, A. P.; Whitwell, T. C.; Sani, M. A.; James, M.; Separovic, F. The Antimicrobial Peptide Aurein 1.2 Disrupts Model Membranes via the Carpet Mechanism. *Phys. Chem. Chem. Phys.* **2012**. https://doi.org/10.1039/c2cp43099a.

(25) Gehman, J. D.; Luc, F.; Hall, K.; Lee, T. H.; Boland, M. P.; Pukala, T. L.; Bowie, J. H.; Aguilar, M. I. and Separovic, F. Effect of Antimicrobial Peptides from Australian Tree Frogs on Anionic Phospholipid Membranes. *Biochemistry* **2008**, *47*, 8557–8565. https://doi.org/10.1021/bi800320v.

(26) Rai, D. K.; Qian, S. Interaction of the Antimicrobial Peptide Aurein 1.2 and Charged Lipid Bilayer. *Sci. Rep.* **2017**. https://doi.org/10.1038/s41598-017-03795-6.

(27) Poger, D.; Pöyry, S.; Mark, A. E. Could Cardiolipin Protect Membranes against the Action of Certain Antimicrobial Peptides? Aurein 1.2, a Case Study. *ACS Omega* **2018**. https://doi.org/10.1021/acsomega.8b02710.

(28) Sharma, V. K.; Qian, S. Effect of an Antimicrobial Peptide on Lateral Segregation of Lipids: A Structure and Dynamics Study by Neutron Scattering. *Langmuir* **2019**. https://doi.org/10.1021/acs.langmuir.8b04158.

(29) McCubbin, G. A.; Praporski, S.; Piantavigna, S.; Knappe, D.; Hoffmann, R.; Bowie, J. H.; Separovic, F.; Martin, L. L. QCM-D Fingerprinting of Membrane-Active Peptides. *Eur. Biophys. J.* **2011**. https://doi.org/10.1007/s00249-010-0652-5.

(30) Ambroggio, E. E.; Separovic, F.; Bowie, J. H.; Fidelio, G. D.; Bagatolli, L. A. Direct Visualization of Membrane Leakage Induced by the Antibiotic Peptides: Maculatin, Citropin, and Aurein. *Biophys. J.* **2005**, *89*, 1874–1881. https://doi.org/10.1529/biophysj.105.066589.

(31) Balatti, G. E.; Martini, M. F.; Pickholz, M. A Coarse-Grained Approach to Studying the Interactions of the Antimicrobial Peptides Aurein 1.2 and Maculatin 1.1 with POPG/POPE Lipid Mixtures. *J. Mol. Model.* **2018**. https://doi.org/10.1007/s00894-018-3747-z.

(32) Yeaman, M. R.; Yount, N. Y. Mechanisms of Antimicrobial Peptide Action and Resistance. *Pharmacological Reviews*. **2003**. https://doi.org/10.1124/pr.55.1.2.

(33) Von Deuster, C. I. E.; Knecht, V. Competing Interactions for Antimicrobial Selectivity Based on Charge Complementarity. *Biochim. Biophys. Acta - Biomembr.* **2011**, *1808*, 2867–2876. https://doi.org/10.1016/j.bbamem.2011.08.005.

(34) Fujii, G.; Eisenberg, D.; Selsted, M. E. Defensins Promote Fusion and Lysis of Negatively Charged Membranes. *Protein Sci.* **1993**. https://doi.org/10.1002/pro.5560020813.

(35) Matsuzaki, K.; Sugishita, K. I.; Harada, M.; Fujii, N.; Miyajima, K. Interactions of an Antimicrobial Peptide, Magainin 2, with Outer and Inner Membranes of Gram-Negative Bacteria. *Biochim. Biophys. Acta - Biomembr.* **1997**. https://doi.org/10.1016/S0005-2736(97)00051-5.

(36) Matsuzaki, K.; Sugishita, K. I.; Ishibe, N.; Ueha, M.; Nakata, S.; Miyajima, K.; Epand, R. M. Relationship of Membrane Curvature to the Formation of Pores by Magainin 2. *Biochemistry* **1998**, *37*, 11856–11863. https://doi.org/10.1021/bi980539y.

(37) Schmidt, N. W.; Wong, G. C. L. Antimicrobial Peptides and Induced Membrane Curvature: Geometry, Coordination Chemistry, and Molecular Engineering. *Current Opinion in Solid State and Materials Science*. **2013**. https://doi.org/10.1016/j.cossms.2013.09.004.

(38) Bayer, A. S.; Prasad, R.; Chandra, J.; Koul, A.; Smriti, M.; Varma, A.; Skurray, R. A.; Firth, N.; Brown, M. H.; Koo, S. P. and Yeaman, M.R. In Vitro Resistance of Staphylococcus Aureus to Thrombin-Induced Platelet Microbicidal Protein Is Associated with Alterations in Cytoplasmic Membrane Fluidity. *Infect. Immun.* **2000**. https://doi.org/10.1128/IAI.68.6.3548-3553.2000.

(39) Schroeder, B. O.; Wu, Z.; Nuding, S.; Groscurth, S.; Marcinowski, M.; Beisner, J.; Buchner, J.; Schaller, M.; Stange, E. F.; Wehkamp, J. Reduction of Disulphide Bonds Unmasks Potent Antimicrobial Activity of Human β 2-Defensin 1. *Nature* **2011**. https://doi.org/10.1038/nature09674.

(40) Seto, G. W. J.; Marwaha, S.; Kobewka, D. M.; Lewis, R. N. A. H.; Separovic, F.; McElhaney, R. N. Interactions of the Australian Tree Frog Antimicrobial Peptides Aurein 1.2, Citropin 1.1 and Maculatin 1.1 with Lipid Model Membranes: Differential Scanning Calorimetric and Fourier Transform Infrared Spectroscopic Studies. *Biochim. Biophys. Acta - Biomembr.* **2007**, *1768*, 2787–2800. https://doi.org/10.1016/j.bbamem.2007.07.018.

(41) Szymanowski, F.; Balatti, G. E.; Ambroggio, E.; Hugo, A. A.; Martini, M. F.; Fidelio, G. D.; Gómez-Zavaglia, A.; Pickholz, M.; Pérez, P. F. Differential Activity of Lytic α-Helical Peptides on Lactobacilli and Lactobacilli-Derived Liposomes. *Biochim. Biophys. acta. Biomembr.* **2019**. https://doi.org/10.1016/j.bbamem.2019.03.004.

(42) Zavaglia, A. G.; Disalvo, E. A.; De Antoni, G. L. Fatty Acid Composition and Freeze-Thaw Resistance in Lactobacilli. *J. Dairy Res.* **2000**, *67*, 241–247. https://doi.org/10.1017/S0022029900004179.

(43) Hugo, A. A.; De Antoni, G. L.; Pérez, P. F. Lactobacillus Delbrueckii Subsp Lactis (Strain CIDCA 133) Resists the Antimicrobial Activity Triggered by Molecules Derived from Enterocyte-like Caco-2 Cells. *Lett. Appl. Microbiol.* **2010**. https://doi.org/10.1111/j.1472-765X.2010.02796.x.

(44) Hugo, A. A.; Tymczyszyn, E. E.; Gómez-Zavaglia, A.; Pérez, P. F. Effect of Human Defensins on Lactobacilli and Liposomes. *J. Appl. Microbiol.* **2012**, *113*, 1491–1497. https://doi.org/10.1111/j.1365-2672.2012.05433.x.

(45) Santo, K. P.; Berkowitz, M. L. Difference between Magainin-2 and Melittin Assemblies in Phosphatidylcholine Bilayers: Results from Coarse-Grained Simulations. *J. Phys. Chem. B* **2012**, *116*, 3021–3030. https://doi.org/10.1021/jp212018f.

(46) Cruz, V. L.; Ramos, J.; Melo, M. N.; Martinez-Salazar, J. Bacteriocin AS-48 Binding to Model Membranes and Pore Formation as Revealed by Coarse-Grained Simulations. *Biochim. Biophys. Acta - Biomembr.* **2013**, *1828*, 2524–2531. https://doi.org/10.1016/j.bbamem.2013.05.036.

(47) Catte, A.; Wilson, M. R.; Walker, M.; Oganesyan, V. S. Antimicrobial Action of the Cationic Peptide, Chrysophsin-3: A Coarse-Grained Molecular Dynamics Study. *Soft Matter* **2018**. https://doi.org/10.1039/c7sm02152f.

(48) Sengupta, D.; Leontiadou, H.; Mark, A. E.; Marrink, S. J. Toroidal Pores Formed by Antimicrobial Peptides Show Significant Disorder. *Biochim. Biophys. Acta - Biomembr.* **2008**. https://doi.org/10.1016/j.bbamem.2008.06.007.

(49) Balatti, G. E.; Martini, M. F.; Pickholz, M. *Insights on the Antimicrobial Peptides Transient Pores Life as Function of the Ratio Glicolipid/Phospholipids on Model Membranes: A Coarse-Grained Molecular Dynamics Simulations Approach. Unpublished Manuscript.*

(50) Touw, W. G.; Baakman, C.; Black, J.; te Beek, T. A. H.; Krieger, E.; Joosten, R. P.; Vriend, G. A Series of PDB-Related Databanks for Everyday Needs. *Nucleic Acids Res.* **2010**.

(51) Marcotte, I.; Wegener, K. L.; Lam, Y. H.; Chia, B. C. S.; De Planque, M. R. R.; Bowie, J. H.; Auger, M.; Separovic, F. Interaction of Antimicrobial Peptides from Australian Amphibians with Lipid Membranes. *Chem. Phys. Lipids* **2003**, *122* (1–2), 107–120. https://doi.org/10.1016/S0009-3084(02)00182-2.

(52) Abraham, M. J.; Murtola, T.; Schulz, R.; Páll, S.; Smith, J. C.; Hess, B.; Lindah, E. Gromacs: High Performance Molecular Simulations through Multi-Level Parallelism from Laptops to Supercomputers. *SoftwareX* **2015**. https://doi.org/10.1016/j.softx.2015.06.001.

(53) Pronk, S.; Páll, S.; Schulz, R.; Larsson, P.; Bjelkmar, P. P.; Apostolov, R.; Shirts, M. R.; Smith, J. C.; Kasson, P. M.; Van Der Spoel, D.; Hess, B. and Lindahl, E. GROMACS 4.5: A High-Throughput and Highly Parallel Open Source Molecular Simulation Toolkit. *Bioinformatics* **2013**, *29*, 845–854. https://doi.org/10.1093/bioinformatics/btt055.

(54) Van Der Spoel, D.; Lindahl, E.; Hess, B.; Groenhof, G.; Mark, A. E.; Berendsen, H. J. C. GROMACS: Fast, Flexible, and Free. *Journal of Computational Chemistry*. **2005**. https://doi.org/10.1002/jcc.20291.

(55) Berendsen, H.J.C; van der Spoel, D. and van Druded, R. GROMACS: A Message-Passing Parallel Molecular Dynamics Implementation. *J. Comput. Chem.* **1995**, *91*, 43-56. https://doi.org/10.1016/0010-4655(95)00042-E.

(56) Hess, B.; Kutzner, C.; Van Der Spoel, D.; Lindahl, E. GRGMACS 4: Algorithms for Highly Efficient, Load-Balanced, and Scalable Molecular Simulation. *J. Chem. Theory Comput.* **2008**, *4*, 435–447. https://doi.org/10.1021/ct700301q.

(57) Huang, J.; Mackerell, A. D. CHARMM36 All-Atom Additive Protein Force Field: Validation Based on Comparison to NMR Data. *J. Comput. Chem.* **2013**. https://doi.org/10.1002/jcc.23354.

(58) Petersen, H. G. Accuracy and Efficiency of the Particle Mesh Ewald Method. *The Journal of Chemical Physics.* **1995**, *103,* 3668-3679. https://doi.org/10.1063/1.470043

(59) Hess, B.; Bekker, H.; Berendsen, H. J. C.; Fraaije, J. G. E. M. LINCS: A Linear Constraint Solver for Molecular Simulations. *J. Comput. Chem.* **1997**. https://doi.org/10.1002/(SICI)1096-987X(199709)18:12<1463::AID-JCC4>3.0.CO;2-H.

(60) Lee, J.; Cheng, X.; Swails, J. M.; Yeom, M. S.; Eastman, P. K.; Lemkul, J. A.; Wei, S.; Buckner, J.; Jeong, J. C.; Qi, Y.; Sunhwan, J.; Pande, V.S.; Case, D.A; Brooks, C.L.; MacKerell, A.D.; Klauda, J.B. and Im, W. CHARMM-GUI Input Generator for NAMD, GROMACS, AMBER, OpenMM, and CHARMM/OpenMM Simulations Using the CHARMM36 Additive Force Field. *J. Chem. Theory Comput.* **2016**. https://doi.org/10.1021/acs.jctc.5b00935.

(61) Nosé, S. A Unified Formulation of the Constant Temperature Molecular Dynamics Methods. *J. Chem. Phys.* **1984**. https://doi.org/10.1063/1.447334.

(62) Hoover, W. G. Canonical Dynamics: Equilibrium Phase-Space Distributions. *Phys. Rev. A* **1985**, *31*, 1695–1697. https://doi.org/10.1103/PhysRevA.31.1695.

(63) Parrinello, M. Polymorphic Transitions in Single Crystals: A New Molecular Dynamics Method. *J. Appl. Phys.* **1981**, *52* , 7182. https://doi.org/10.1063/1.328693.

(64) Sun, D.; Forsman, J.; Woodward, C. E. Amphipathic Membrane-Active Peptides Recognize and Stabilize Ruptured Membrane Pores: Exploring Cause and Effect with Coarse-Grained Simulations. *Langmuir* **2015**. https://doi.org/10.1021/la5038266.

(65) Ramírez, P. G.; Del Pópolo, M. G.; Vila, J. A.; Szleifer, I.; Longo, G. S. Adsorption and Insertion of Polyarginine Peptides into Membrane Pores: The Trade-off between Electrostatics, Acid-Base Chemistry and Pore Formation Energy. *J. Colloid Interface Sci.* **2019**. https://doi.org/10.1016/j.jcis.2019.05.087.

(66) Albano, J. M. R.; Mussini, N.; Toriano, R.; Facelli, J. C.; Ferraro, M. B.; Pickholz, M. Calcium Interactions with Cx26 Hemmichannel: Spatial Association between MD Simulations Biding Sites and Variant Pathogenicity. *Comput. Biol. Chem.* **2018**. https://doi.org/10.1016/j.compbiolchem.2018.11.004.

(67) Wood, I.; Martini, M. F.; Pickholz, M. Similarities and Differences of Serotonin and Its Precursors in Their Interactions with Model Membranes Studied by Molecular Dynamics Simulation. *J. Mol. Struct.* **2013**. https://doi.org/10.1016/j.molstruc.2013.04.011.

(68) Begum, P.; Madhavi, G.; Rajagopal, S.; Viswanath, B.; Razak, M.; Venkataratnamma, V. Probiotics as Functional Foods: Potential Effects on Human Health and Its Impact on Neurological Diseases. *International Journal of Nutrition, Pharmacology, Neurological Diseases*. **2017**. https://doi.org/10.4103/ijnpnd.ijnpnd_90_16.

(69) Parvez, S.; Malik, K. A.; Ah Kang, S.; Kim, H. Y. Probiotics and Their Fermented Food Products Are Beneficial for Health. *Journal of Applied Microbiology*. Petersen, H. G. Accuracy and Efficiency of the Particle Mesh Ewald Method. *The Journal of Chemical Physics*. **1995**, *103,* 3668-3679. https://doi.org/10.1063/1.470043. https://doi.org/10.1111/j.1365-2672.2006.02963.x.

(70) Nagpal, R.; Kumar, A.; Kumar, M.; Behare, P. V.; Jain, S.; Yadav, H. Probiotics, Their Health Benefits and Applications for Developing Healthier Foods: A Review. FEMS Microbiology Letters. Petersen, H. G. Accuracy and Efficiency of the Particle Mesh Ewald Method. *The Journal of Chemical Physics*. **1995**, *103,* 3668-3679. https://doi.org/10.1063/1.470043. https://doi.org/10.1111/j.1574-6968.2012.02593.x.

(71) Hill, C.; Guarner, F.; Reid, G.; Gibson, G. R.; Merenstein, D. J.; Pot, B.; Morelli, L.; Canani, R. B.; Flint, H. J.; Salminen, S.; Calder, P.C and Sanders, M.E. Expert Consensus Document: The International Scientific Association for Probiotics and Prebiotics Consensus Statement on the Scope and Appropriate Use of the Term Probiotic. *Nat. Rev. Gastroenterol. Hepatol.* **2014**. https://doi.org/10.1038/nrgastro.2014.66.

(72) Plaza-Diaz, J.; Ruiz-Ojeda, F. J.; Gil-Campos, M.; Gil, A. Mechanisms of Action of Probiotics. In *Advances in Nutrition*; **2019**. https://doi.org/10.1093/advances/nmy063.

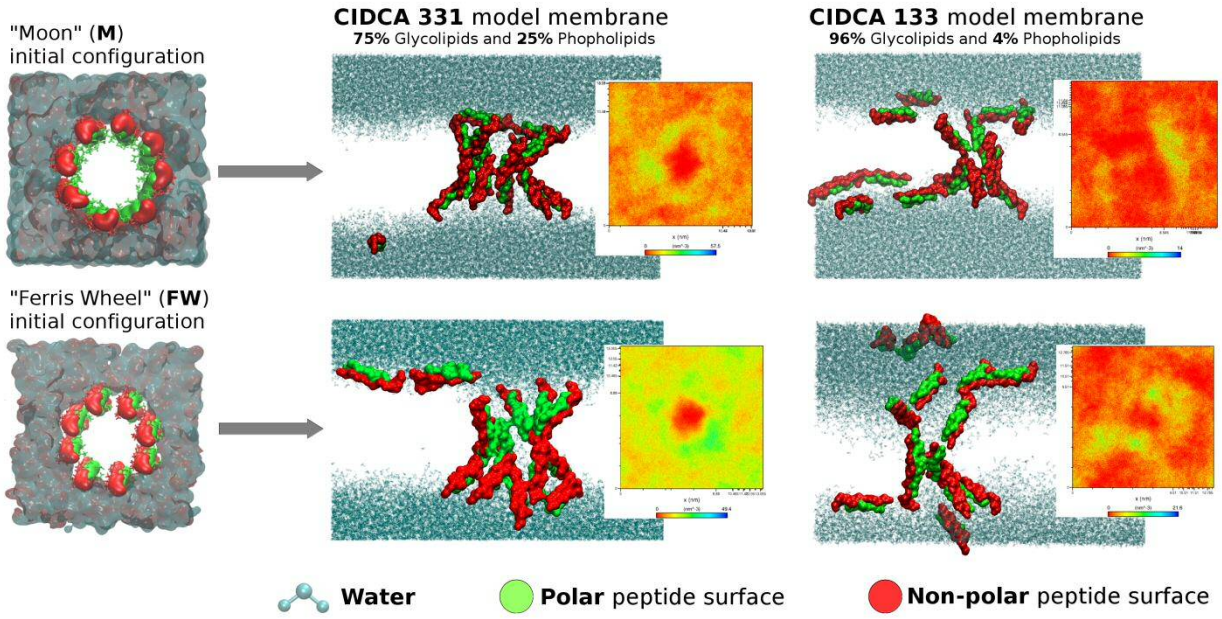

For Table of Contents Use Only

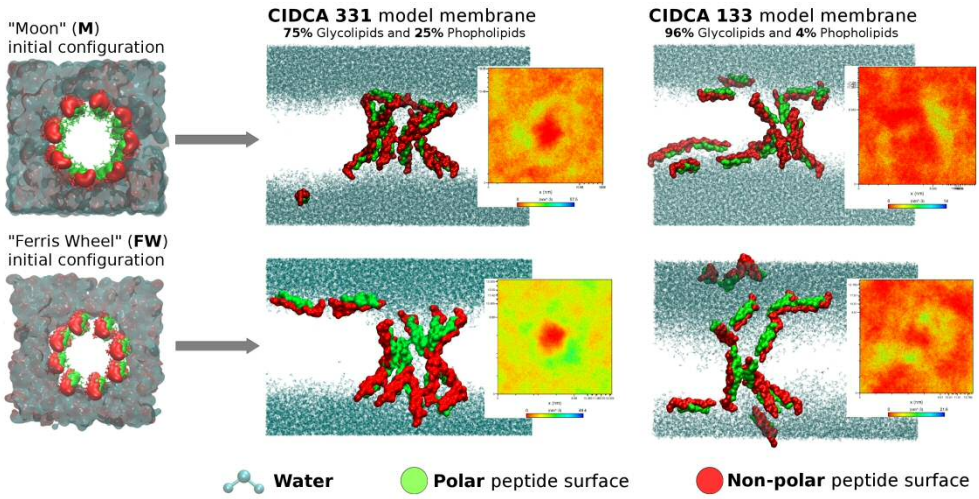

240x129mm (300 x 300 DPI)